AD-A161 758 CHAOS AND NONLINEAR DYNAMICS OF SINGLE-PARTICLE ORBITS IN A MAGNETOTAIL-LIKE MAGNETIC FIELD(U) NAVAL RESEARCH LAB WASHINGTON DC J CHEN ET AL. 22 NOV 85 NRL-MR-5665 1/1

UNCLASSIFIED F/G 4/1 NL

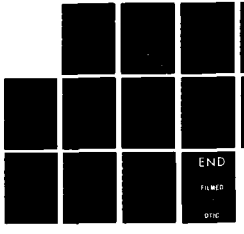

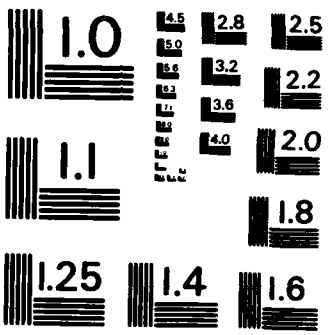

MICROCOPY RESOLUTION TEST CHART
NATIONAL BUREAU OF STANDARDS-1963-A

NRL Memorandum Report 5665

Chaos and Nonlinear Dynamics of Single-Particle Orbits in a Magnetotail-like Magnetic Field

J. CHEN AND P. J. PALMADESSO

Geophysical and Plasma Dynamics Branch
Plasma Physics Division

November 22, 1985

This research was supported by the National Aeronautics and Space Administration and the Office of Naval Research.

NAVAL RESEARCH LABORATORY
Washington, D.C.

SECURITY CLASSIFICATION OF THIS PAGE

AD-A161750

REPORT DOCUMENTATION PAGE

1a REPORT SECURITY CLASSIFICATION UNCLASSIFIED	1b RESTRICTIVE MARKINGS
2a SECURITY CLASSIFICATION AUTHORITY	3 DISTRIBUTION / AVAILABILITY OF REPORT
2b DECLASSIFICATION / DOWNGRADING SCHEDULE	Approved for public release; distribution unlimited.
4 PERFORMING ORGANIZATION REPORT NUMBER(S) NRL Memorandum Report 5665	5 MONITORING ORGANIZATION REPORT NUMBER(S)
6a NAME OF PERFORMING ORGANIZATION Naval Research Laboratory 6b OFFICE SYMBOL (If applicable) Code 4780	7a. NAME OF MONITORING ORGANIZATION
6c ADDRESS (City, State, and ZIP Code) Washington, DC 20375-5000	7b. ADDRESS (City, State, and ZIP Code)
8a. NAME OF FUNDING / SPONSORING ORGANIZATION ONR and NASA 8b. OFFICE SYMBOL (If applicable)	9. PROCUREMENT INSTRUMENT IDENTIFICATION NUMBER
8c ADDRESS (City, State, and ZIP Code) Arlington, VA 22217 Washington, DC 20546	10 SOURCE OF FUNDING NUMBERS PROGRAM ELEMENT NO (See page ii) / PROJECT NO. / TASK NO. / WORK UNIT ACCESSION NO.

11 TITLE (Include Security Classification)

Chaos and Nonlinear Dynamics of Single-Particle Orbits in a Magnetotail-like Magnetic Field

12 PERSONAL AUTHOR(S)
Chen, J. and Palmadesso, P.J.

13a TYPE OF REPORT	13b TIME COVERED	14. DATE OF REPORT (Year, Month, Day)	15. PAGE COUNT
Interim	FROM _____ TO _____	1985 November 22	30

16 SUPPLEMENTARY NOTATION This research was supported by the National Aeronautics and Space Administration and the Office of Naval Research.

17 COSATI CODES			18 SUBJECT TERMS (Continue on reverse if necessary and identify by block number)
FIELD	GROUP	SUB-GROUP	Chaos, Magnetotail Hamiltonian dynamics, Quasi-neutral sheet

19 ABSTRACT (Continue on reverse if necessary and identify by block number)

The properties of charged-particle motion in Hamiltonian dynamics are studied in a magnetotail-like magnetic field configuration. It is shown by numerical integration of the equation of motion that the system is generally nonintegrable and that the particle motion can be classified into three distinct types of orbits; the bounded integrable orbits, unbounded stochastic orbits and unbounded transient orbits. It is also shown that different regions of the phase space exhibit qualitatively different response to external influences. The concept of "differential memory" in single-particle distributions is proposed. Physical implications to the dynamical properties of the magnetotail plasmas, and the possible generation of non-Maxwellian features in the distribution function are discussed.

20 DISTRIBUTION / AVAILABILITY OF ABSTRACT	21 ABSTRACT SECURITY CLASSIFICATION
☒ UNCLASSIFIED/UNLIMITED ☐ SAME AS RPT ☐ DTIC USERS	UNCLASSIFIED
22a NAME OF RESPONSIBLE INDIVIDUAL J. D. Huba	22b TELEPHONE (Include Area Code) (202) 767-3630 / 22c. OFFICE SYMBOL Code 4780

DD FORM 1473, 84 MAR 83 APR edition may be used until exhausted
All other editions are obsolete

SECURITY CLASSIFICATION OF THIS PAGE

10. SOURCE OF FUNDING NUMBERS

PROGRAM ELEMENT NO.	PROJECT NO.	TASK NO.	WORK UNIT ACCESSION NO.
61153N	RR033-02-44 W-15494		DN380-475 DN430-607

CONTENTS

CHAOS AND NONLINEAR DYNAMICS OF SINGLE-PARTICLE ORBITS IN A MAGNETOTAIL-LIKE MAGNETIC FIELD

I. INTRODUCTION

It has long been realized that a complete understanding of the properties of the earth's magnetotail requires an understanding of the charged-paticle motion. The quiet-time magnetotail field may be modeled, in its simplest form, by a neutral sheet magnetic profile $B_o(z)\hat{x}$ with a superimposed normal field $B_n\hat{z}$ (the so-called "quasi-neutral sheet" geometry). Figure 1 gives a schematic drawing of such a magnetic configuration and the coordinate system. A considerable amount of work already exists, dealing with a number of specialized aspects of the particle motion. The methods used include approximate analytical methods (Speiser, 1965; Alexeev and Kropotkin, 1970; Sonnerup, 1971; Stern and Palmadesso, 1975; Pellat and Schmidt, 1979) and numerical methods (Speiser, 1967; Cowley, 1973; Eastwood, 1972; Swift, 1977). More recently, Wagner et al. (1979) performed a numerical study encompassing the previously studied orbits.

In all of the previous works, the underlying implicit concept is that the particle motion in a quasi-neutral sheet is ultimately regular and integrable. In this paper, we demonstrate that charged-particle motion in a quasi-neutral sheet is nonintegrable because of the normal magnetic field component. Recent developments in nonlinear dynamics (see, for example, Lichtenberg and Lieberman, 1983) have led to important and novel insights into the physical properties of dynamical systems. For the system of interest here, i.e. the magnetotail, we find that the phase space structure of the particle orbits can yield important information regarding the long-time plasma properties of the system not available via the conventional approach. For example, we find that particle motions can be classified into three distinct major types of orbits; the bounded integrable orbits, unbounded stochastic orbits and unbounded transient orbits. The existence of distinct classes of orbits has profound effects on the plasma particle distribution and on the response of the magnetotail to external influences.

Manuscript approved July 30, 1985.

Moreover, the distribution and character of the charged-particle orbits can have a significant impact on other dynamical properties of the magnetotail. One important example is the tearing-mode instability (Furth, 1962; Pfirsch, 1962; Laval et al., 1966) which has long been thought to play an important role in magnetic field reconnection (Coppi et al, 1966; Schindler, 1966). It has recently been shown that the theoretically predicted growth rates of the collisionless tearing instability can be increased dramatically by the presence of temperature anisotropy or other non-Maxwellian features in the particle distribution (Chen and Palmadesso, 1984; Chen et al., 1984; Chen and Lee, 1985). In particular, the growth rate can be enhanced in excess of a few orders of magnitude and the wavelengths of the fastest growing modes are shortened significantly. As will be seen in the following sections, there is a close connection between the topology of the magnetotail magnetic field and the properties of particle distribution functions which can persists in the tail for more than a few transit times. A fundamental question, then, is whether the magnetotail can sustain free-energy carrying non-Maxwellian features that can support large-scale instabilities of potential relevance to magnetotail dynamics, such as the anisotropic collisionless tearing mode. Thus, it is desirable to gain a better understanding of the way in which magnetic field topology affects magnetotail particle distribution functions.

The treatment given in this paper is applicable to both ions and electrons. However, we will primarily refer to the ion motion for illustration. The modifications needed for electrons are trivial. The emphasis of the paper will be on the physical properties, rather than the mathematics.

II. The Model

In order to model the motion of charged particles in the magnetotail, we consider a magnetic field given by $\underline{B} = B_o f(z)\hat{\underline{x}} + B_n\hat{\underline{z}}$, where B_o is the asymptotic field in the x direction, B_n is the uniform normal field and $B_o f(z)$ is a neutral sheet profile such that $f(-z) = -f(z)$. In this paper, we primarily use the Harris configuration (see, for example, Wagner et al., 1979)

$$f(z) = \tanh(z/\delta), \tag{1}$$

where δ is the characteristic scale length of the magnetic field. This field configuration and the coordinate system are schematically shown in Figure 1. For convenience, we also use s to indicate the distance from the $z = 0$ plan along field lines; parallel to $\underline{B}$, we have $s \to +\infty$ as $z \to +\infty$, and, anti-parallel to $\underline{B}$, we have $s \to -\infty$ as $z \to -\infty$. The treatment is also applicable to other quasi-neutral sheet configurations and another example, $f(z) = z/\delta$, will be discussed.

We choose the gauge such that the vector potential is

$$A_y(x,z) = - B_o F(z) + B_n x$$

where $dF(z)/dz = f(z)$. For the model field of equation (1),

$$F(z) = \delta \ln[\cosh(z/\delta)].$$

The single-particle motion is described by the equation of motion

$$m\frac{d\underline{v}}{dt} = \frac{q}{c}\underline{v} \times \underline{B} \tag{2}$$

This vector equation possesses three exact constants of motion; the Hamiltonian $H = mv^2/2$ where $v^2 = v_x^2 + v_y^2 + v_z^2$, the canonical momentum $P_y = mv_y + (q/c)A_y(x,z)$ and a constant $C_x = m(v_x - \Omega_n y)$ associated with the x-motion. In this paper, we will use $\Omega_n = qB_n/mc$ and $\Omega_o = qB_o/mc$ for each species. However, we note the following previously unrealized but important property. If we consider the Poisson brackets of the constants of motion, we find $[H, P_y] = 0$ and $[H, C_x] = 0$, as they should be. However, for C_x and P_y, we find

$$[C_x, P_y] = - m\Omega_n \tag{3}$$

so that C_x and P_y are not in involution. Thus the system is likely to possess nonintegrable, stochastic orbits. This is in fact the case as will be demonstrated in this paper. As a general remark, this conclusion is due to the existence of the normal magnetic field component in the null region and is not limited to the particular choice of equation (1) or the gauge.

We first consider a number of general properties of the particle motion. It is easy to show that the motion in the x-z plane can be described by an effective potential given by

$$\Gamma(x, z) = \frac{1}{2m}[P_y - \frac{q}{c}A_y(x, z)]^2, \tag{4}$$

so that $md^2x/dt^2 = -\partial\Gamma/\partial x$ and $md^2z/dt^2 = -\partial\Gamma/\partial z$. It is also easy to see that the magnetic field lines and the constant - Γ lines have the same geometrical shapes in the x-z plane (see Figure 1).

It is convenient to express equation (2) in the dimensionless component form:

$$\frac{d^2X}{d\tau^2} = \frac{dY}{d\tau}, \tag{5}$$

$$\frac{d^2Y}{d\tau^2} = \frac{d}{d\tau}\{b_n^{-2}\ln[\cosh(b_nZ)] - X\}, \tag{6}$$

and

$$\frac{d^2Z}{d\tau^2} = -b_n^{-1}\tanh(b_nZ)\frac{dY}{d\tau}, \tag{7}$$

where the normalized variables are $b_n \equiv B_n/B_o$, $X \equiv (x - P_y/m\Omega_n)/b_n\delta$, $Y \equiv (y + C_x/m\Omega_n)/b_n\delta$, $Z \equiv z/b_n\delta$ and $\tau = \Omega_n t$. The normalized Hamiltonian is then $\hat{H} \equiv H/(mb_n^2\Omega_n^2\delta^2)$. If we use the magnetic field $f(z) = z/\delta$, the ratio b_n can be normalized away completely, indicating that all parabolic field lines can be scaled to any other parabola. In general, a solution of equations (5) - (7) represents a set of orbits corresponding to different choices of P_y and C_x.

The above system of equations (5)-(7) is invariant under the replacement $Z \to -Z$. In addition, the system also remains invariant under the simultaneous replacement $Y \to -Y$ and $\tau \to -\tau$. Because of energy conservation, the normalized velocity components $V_x \equiv dX/d\tau$, $V_y \equiv dY/d\tau$ and $V_z \equiv dZ/d\tau$ are limited to the range of $-(2\hat{H})^{1/2}$ to $+(2\hat{H})^{1/2}$. In addition, the coordinate Y is limited to $|Y| \leq (2\hat{H})^{1/2}$ and X ranges from $b_n^{-2}\ln[\cosh(b_nZ)] - (2\hat{H})^{1/2}$ to $b_n^{-2}\ln[\cosh(b_nZ)] + (2\hat{H})^{1/2}$ at any given Z. However, for a given orbit, X and Z need not be limited.

Further insight inito the particle motion is obtained by considering small oscillations ($|z| \ll \delta$) about $Z = 0$. The z-motion can then be described by the Mathieu equation:

$$\frac{d^2Z}{d\tau^2} + [-(2\hat{H})^{1/2}\cos(\tau)]Z = 0. \tag{8}$$

This shows that the small oscillation motion can be stable or unstable depending only on H. Most small oscillations turn out to be unstable. We note that stable small oscillation manifests itself as essentially magnetized, integrable orbits. As an example, we find $\hat{H} \lesssim 0.10$ corresponds to stable oscillations about $Z = 0$.

III. RESULTS

The system of equations (5)-(7) is solved by numerical integration. A useful technique for displaying the long-time properties of the particle motion is to use the Poincare surface of section method (see, for example, Lichtenberg and Lieberman, 1983). Figure 2(a) shows the surface of section plot for $\hat{H} = 500$ and $b_n = 0.1$, evaluated at $Z = 0$. All kinematically allowable orbits are confined within the circle of $(2\hat{H})^{1/2}$. Each point represents the coordinates X and $\dot{X} \equiv dX/d\tau$ at the point where the orbit crosses the $Z = 0$ plane. Since a given point at $Z = 0$ corresponds to two orbits, one with $\dot{Z} > 0$ and the other with $\dot{Z} < 0$, which are mirror images of each other, crossings from both above and below the $Z = 0$ plane are included. The regions C1 through C5 are, of course, fully populated with orbits and they will be discussed in the following paragraphs.

The orbits in the region marked A are bounded and integrable. Several sample integrable orbits are indicated. Evidently, there is a third independent constant of motion in this region. In the present system, an integrable orbit densely covers a two-dimensional hypersurface whose cross-section through $Z = 0$ is represented by a closed curve. In the absence of any noise, the orbit remains on the hypersurface indefinitely. The figure also clearly demonstrates that there is a large stochastic region, marked

B, where the orbits are sensitive to the initial condition. The stochastic region is disjoint from the integrable region A; that is, there is no orbit that can connect the two regions.

The model system described by equation (1) is unusual in that all non-integrable orbits eventually escape to infinity so that the stochastic region is actually covered by infinitely many orbits, each one crossing the Z = 0 plane a finite number of times. The non-integrable orbits may be thought of as originating from infinity and escaping to infinity. However, region B cannot be accessed from infinity directly. All orbits at infinity that can reach Z = 0 are mapped into region C1. The orbits then successively cross regions C2 through C5. After crossing C5, some orbits enter the stochastic region B. That is, region B can only be accessed from region C5. The regions C1 through C5 in turn have interesting substructures, as shown in Figure 2(b). The orbits in C1 between regions S1 and T1 are those which originate from infinity, successively re-cross the plane in regions C2, C3, C4 and C5. From C5, they escape to infinity. The orbits in the small region to the left of T1 also re-cross the plane in regions C2, C3 and C4, above T2, T3 and T4, respectively, but they escape to infinity from the subregion of C4 above T4. These orbits which will be referred to as transient orbits do not exhibit noticeable stochastic behavior. Only orbits of this type are shown in Figure 2(b).

An orbit entering S1 makes successive crossings in regions S2 through S5, from which it enters region B where it makes a finite number of crossings. It then enters one of the hashed regions before escaping to infinity. Orbits in T1 behave in a similar manner. All orbits in region B eventually wonder into the hashed regions and escape. We emphasize that no orbit enters regions C1 through C5 from the stochastic region B. Needless to say, the integrable region cannot be accessed from infinity. Thus, in the coordinates X, Y, and Z, one can visualize the orbits as forming two flux tubes, one from $+\infty$ and the other from $-\infty$, which are mirror images of each other. The bulk of each flux tube, consisting of transient orbits, simply threads the neutral plane (Z = 0) and extends to infinity. The orbits in the two regions of the flux tube corresponding to S1 and T1 separate from the flux tube, execute stochastic motion in region B and rejoins the flux tube through the hashed regions. Before entering C5 or

after leaving the hashed regions, the orbits do not exhibit noticeable stochastic behavior. Indeed, in traversing the system via C1 through C5, transient and stochastic orbits are similar in appearance. Note that the different types of orbits spend significantly different lengths of time in the vicinity of the neutral plane before escaping to infinity.

Similar structures exist in the surfaces of section for different values of $\hat{H}$. Figure 3(a) shows the plot for $\hat{H} = 50$. The "blank" regions are analogous to the regions C1 through C5 of Figure 2(a), containing structures similar to those described in Figure 2(b). In Figure 3(b), we show the surface of section plot for $\hat{H} = 7$. In general, as the value of $\hat{H}$ is reduced, large-scale integrable regions become more fragmented and complicated. For $\hat{H} \lesssim 6.2$, large integrable regions vanish and essentially all orbits are of the stochastic or the transient types. However, there may be small-scale integrable regions not resolvable in these figures. Figure 3(c) shows the plot for $\hat{H} = 0.25$. In this case, the transient orbits cross the $Z = 0$ plane only once. In Figure 3(d), we show the surface of section for $\hat{H} = 1.184 \times 10^{-2}$. In this case, the orbits near the outer edge of the circle execute small oscillations in the Z direction as described by equation (8). This value of $\hat{H}$ corresponds to stable oscillation. Thus, these orbits are essentially integrable and adiabatic as shown by the figure. Closer in to the center of the circle, the small oscillation approximation evidently breaks down and the motion is stochastic. In general, as the value of $\hat{H}$ is decreased, larger fractions of the allowed surfaces of section will be occupied by the adiabatic orbits executing small oscillations. Note that, for any $\hat{H}$, the outer most allowable orbit, i.e., $\dot{X}^2 + X^2 = 2\hat{H}$, has $\dot{Z} = 0$ and is an integrable orbit.

It is possible to estimate the number of times the flux tube crosses the $Z = 0$ plane. The orbits in the flux tube have the typical orbital size given by $d = (2\rho\delta)^{1/2}$ near $Z = 0$ (Chen and Palmadesso, 1984; Chen et al., 1984) where ρ is the Larmour radius of a particle with the Hamiltonian $\hat{H}$ in the field B_o. Then, it is easy to show

$$\frac{d}{\delta} = (8b_n^4\hat{H})^{1/4}.$$

Since the Y-range is limited to $(2\hat{H})^{1/2}$, we see that there should be

$$N \sim (\hat{H}/2)^{1/4} + 1, \tag{9}$$

where N is the number of crossing points for a given value of $\hat{H}$. Here, N is to be understood as an integer. For example, if $\hat{H} = 500$, then N = 5 as shown by Figure 2(a). For $\hat{H} = 7$, we have N = 2. For $\hat{H} \ll 2$, N must remain equal to unity. We have found the formula to be accurate for a wide range of $\hat{H}$, although it tends to underestimate the actual number of crossings slightly for very high values of $\hat{H}$. Note that the number of crossings for stochastic orbits can range from a few crossings to hundreds of crossings, corresponding to a wide range of time the orbits spend in the vicinity of the Z = 0 plane.

At the center of an integrable region is a fixed point, which is mapped into itself after a finite number of iterations of the mapping, equations (5) - (7). A fixed point occurring on the axis $\dot{X} = 0$ is mapped into itself by each iteration of the mapping. For example, for $\hat{H} = 500$ (Figure 2(a)), a fixed point occurs at X = 22.591 and $\dot{X} = 0$. Figure 4(a) provides a three-dimensional drawing of the orbit. Fixed points occurring off the axis have higher periods and the orbits cross Z = 0 more than once. Another type of orbits of interest are of the transient type. Figure 4(b) gives a drawing of the orbit which crosses region C1 at X = 0 and $\dot{X} = -26$ (see Figure 2(a)).

From the symmetry properties of equations (5) - (7), it is easy to show that a fixed-point of any orbit is symmetric about Y = 0 because it closes onto itself. In addition, orbits associated with fixed points on $\dot{X} = 0$ are also symmetric about Z = 0. Moreover, it can be shown that the integrable regions (Z = 0) are symmetric about $\dot{X} = 0$ (i.e., Y = 0). The integrable orbits themselves, however, are not symmetric except for the fixed-point orbits.

In Figure 5, we show a surface of section plot for the field configuration given by $f(z) = z/\delta$. In this system, all the field lines are parabolic and the ratio b_n can be scaled away completely from the equation of motion. In this figure, $\hat{H} = 500$ and the plot shows features similar to those in Figure 2(a). The plots corresponding to other values of $\hat{H}$ in Figures 3(a) - 3(d) also have similar features. The primary difference of

this system with the Harris-type system (equation (1)) is that the field lines remain parabolic for all Z so that essentially all orbits are eventually reflected. In constructing this plot, we have imposed an artificial cutoff condition in order to limit computing time, typically corresponding to τ of the order of 5000 and maximum Z of roughly 300. As the cutoff time is increased, reflection from greater maximum Z is included and the "blank" regions decrease in size. In the limit of infinite cutoff time, we believe that each "blank" region diminishes to a point corresponding to the orbit that can indeed reach infinity for each value of $\hat{H}$. These orbits are somewhat analogous to the trajectories passing through the origin of a dipole field (Störmer, 1955). The stochastic region is then covered by a single orbit and the parabolic system contains no true loss-cone. However, the orbits can extend to large Z values so that a given orbit in this phase of its motion may be regarded as having escaped the system for all practical purposes. For the parabolic field case, the large integrable regions also vahish for $\hat{H} \lesssim 6.2$ as in the Harris-type case.

It is possible to understand the previous results in a more unified fashion. Wagner et al. (1979), the most comprehensive of the previous studies, examined only a small number of possible orbits for certain values of the normalized Hamiltonian: $\hat{H}$ = 0.005, 0.0118, 0.5, and 5000. The surface of section technique describes all possible orbits for each value of $\hat{H}$. Wagner et al. (1979) also noticed that, for certain initial conditions, neighboring initial orbits can diverge rapidly. In view of the present work, we now understand this sensitive dependence on initial conditions as a typical property of stochastic motion. Swift (1977) also noted that some orbits appeared to randomize in the Z = 0 plane after a few crossings. This is also typical of stochastic orbits such as those shown in Figures 2 and 3. Our present work provides a more complete understanding of the fundamental nature of the particle motion in the quasi-neutral sheet geometry.

IV. DISCUSSION AND PHYSICAL IMPLICATIONS

A prominent and hitherto unrealized feature is the existence of three distinct and disjoint regions in the phase space, each region consisting of

orbits of distinct nature; (1) bounded integrable orbits, (2) unbounded stochastic orbits and (3) unbounded transient orbits. This behavior is a consequence of the fact that, due to the presence of the z-component of the magnetic field, the system does not possess three global constants of motion which are in involution. We have presented surface of section plots to describe the long-time properties of particle orbits. The various distinct regions of the phase space for two model systems have been discussed in detail. The ergodic hypothesis is false for the magnetotail-like field configuration. We have also identified the flux-tube structure showing the manner in which different regions of the phase space are connected to infinity. One unique feature of the Harris-type system is that all non-integrable orbits extend from infinity to infinity via the Z = 0 plane. Therefore, the stochastic regions consist of infinitely many orbits, each having measure zero. For the parabolic field, no loss-cone appears to exist and one orbit can cover the stochastic region. However, a stochastic orbit can extend to large distances ($|Z| >> \delta$) so that, for all practical purposes, it can reach the external regions. In a physical system such as the magnetotail, the "external" regions may include the magnetopause or the ionosphere.

As described earlier, the transient orbits do not exhibit significant stochasticity. Two adjacent orbits remain adjacent and two adjacent neighborhoods of transient orbits remain adjacent but disjoint. This implies that the transient orbits can carry information from the distant regions. The time a transient orbit spends in the vicinity of the Z = 0 plane is roughly proportional to $\tau_1 \equiv (\Omega_0^{-1}\hat{H}^{1/4})$. The stochastic orbits separate from the transient orbits after finite numbers of crossings, covering the stochastic regions. Thus, the information carried from infinity is randomized after a few crossings. The integrable regions are, of course, not connected to infinity.

Based on the new understanding of the nature of particle orbits in the magnetotail-like field configuration, we suggest the following scenario. Suppose the system contains a population of charged particles in thermal (i.e. Maxwellian) equilibrium. In the absence of noise fields, the different types of orbits remain distinct. There must also be a steady supply of particles in the distant regions to maintain equilibrium. If the

parameters of the distant plasma distribution are changed, then the fact the orbits are divided into distinct types belonging to disjoint regions of the phase space results in a highly non-Maxwellian distribution: After reaching the plane, the particles in the transient-orbit regions replace the existing distribution of particles, thus erasing the memory of the initial distribution on the time scale proportional to τ_1. For the stochastic orbits, the memory of the initial distribution and the information regarding the new external conditions are randomized on the time scale corresponding to several crossings of the plane. The integrable orbits carry the memory of the initial distribution indefinitely as long as the magnetic field remains unchanged. Thus, the three distinct regions respond to changes with different processes and time scales. If noise fields are introduced, then mixing of different regions can occur on yet another time scale, which depends on the amplitudes of the noise fields. We refer to the above process as "differential memory". Clearly, the new distribution is highly non-Maxwellian. The phase space structures as shown by the surface of section plots provide specific clues regarding how the changes in the external regions affect the distributions in the quasi-neutral sheet.

In the context of the earth's magnetotail, it is believed that the collisionless tearing instability may play an important role in reconnection processes. In the usual consideration based on an isotropic neutral sheet, the growth rate is found to be slow in comparison with the relevant time scales such as the time delay which precedes the onset of substorms. However, it has recently been shown (Chen and Palmadesso, 1984; Chen and Lee, 1985) that the growth rate of the collisionless tearing mode in anisotropic or non-Maxwellian neutral sheets can be substantially greater, by a few orders of magnitude, than in the isotropic case due to the mirror forces which are exactly cancelled in an isotropic distribution. Based on the findings of the present work, we consider the possible influence of particle dynamics on the plasma dynamics. If the magnetotail initially in thermal equilibrium is subjected to changes in external conditions, e.g., conditions of IMF, magnetopause, etc., then the discussion above suggests that the magnetotail plasma may develop non-Maxwellian features which can render the magnetotail plasma strongly unstable to the collisionless tearing instability. This process may

manifest itself as rapid reconnection following changes in IMF conditions. We add, however, that the above discussion does not take into account the possible stabilizing influence of the normal magnetic field on the instability itself under certain circumstances (Lembege and Pellat, 1982). This point warrants further consideration and will be addressed in a separate paper.

As we have seen, the particle distribution in the tail-like system is determined by many complicated dynamical properties of particle motion. In this regard, it is important and informative to realize the distinct nature of the three regions in the phase space. Suppose an observer measures the properties of a distribution of particles at some point in a system such as the model system. It is then possible to construct an inverse mapping from the observation to the phase space and identify the type and nature of the orbits. Thus, the surface of section plots may be helpful in organizing observational results.

Finally, we point out that the above results and discussions are based on single-particle motion. In order to determine more quantitavely the nature and associated time scales of these processes, it is necessary to follow an ensemble of particles. This work is currently underway.

Acknowledgments

It is a pleasure to acknowledge enlightening discussions with Dr. G. Schmidt, Dr. Y.C. Lee, Dr. J.M. Finn and Dr. H. Mitchell.

This research was supported by the National Aeronautics and Space Administration and the Office of Naval Research

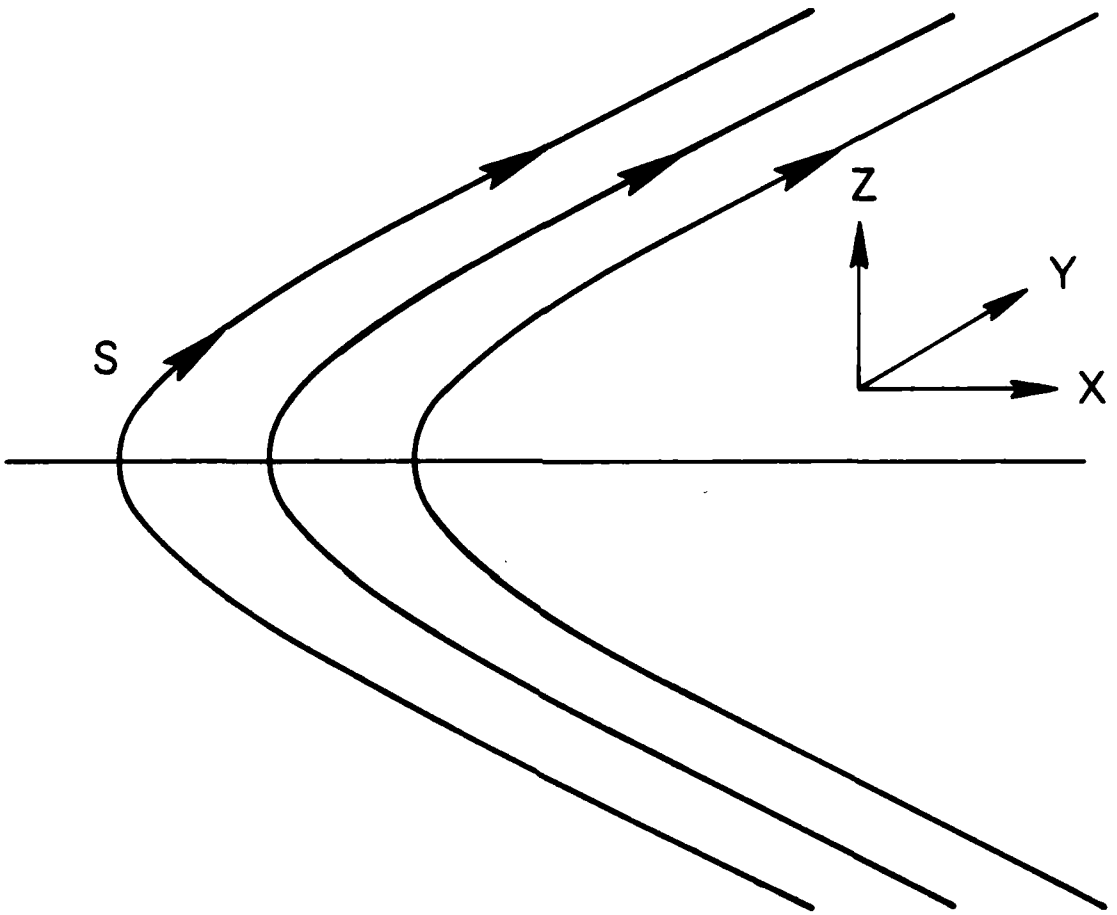

Fig. 1. Schematic drawing of the Harris-type magnetic field (equation (1)) and the coordinate system. The line segment s measures the distance from Z = 0 along the magnetic field lines.

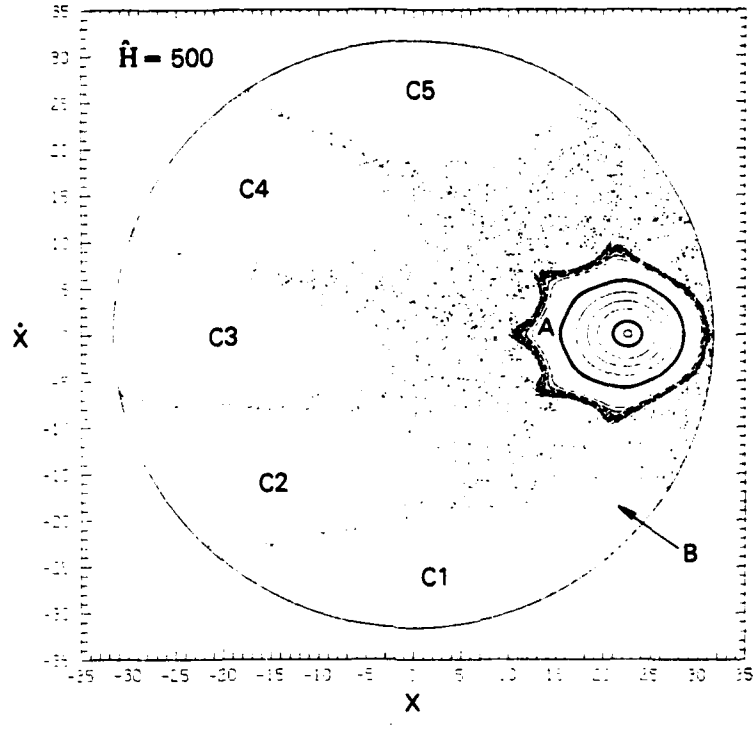

(a)

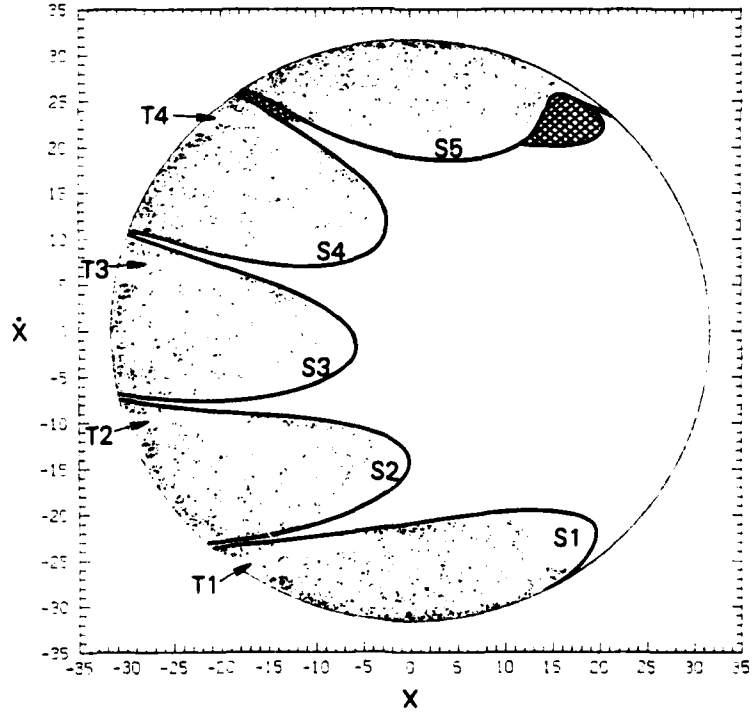

(b)

Fig. 2. Surface of section plots for the Harris-type field with $b_n = 0.1$ and $\hat{H} = 500$. (a)Representative integrable orbits in region A and stochastic orbits in region B. 60000 points. (b)Transient orbits, showing the substructures in regions C1 through C5. 42000 points.

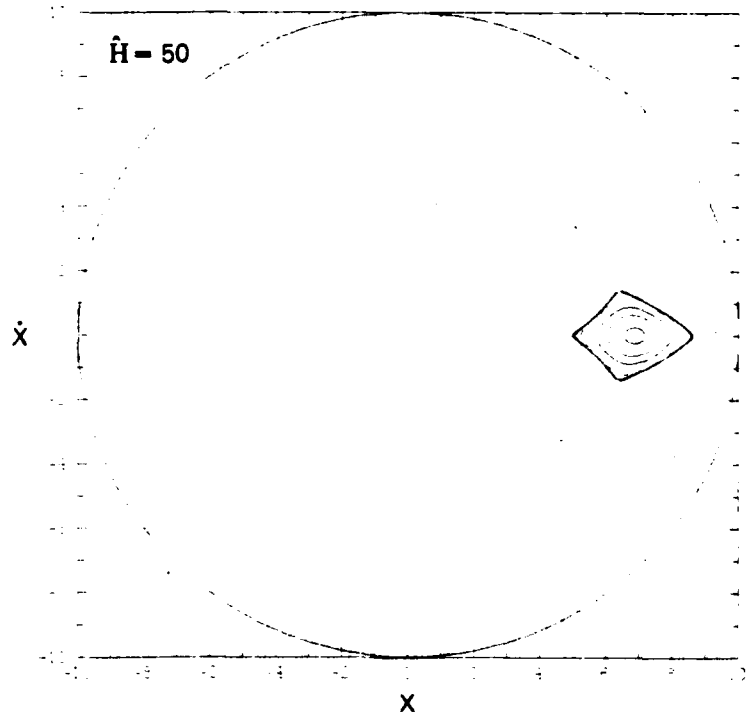

(a) $\hat{H} = 50$

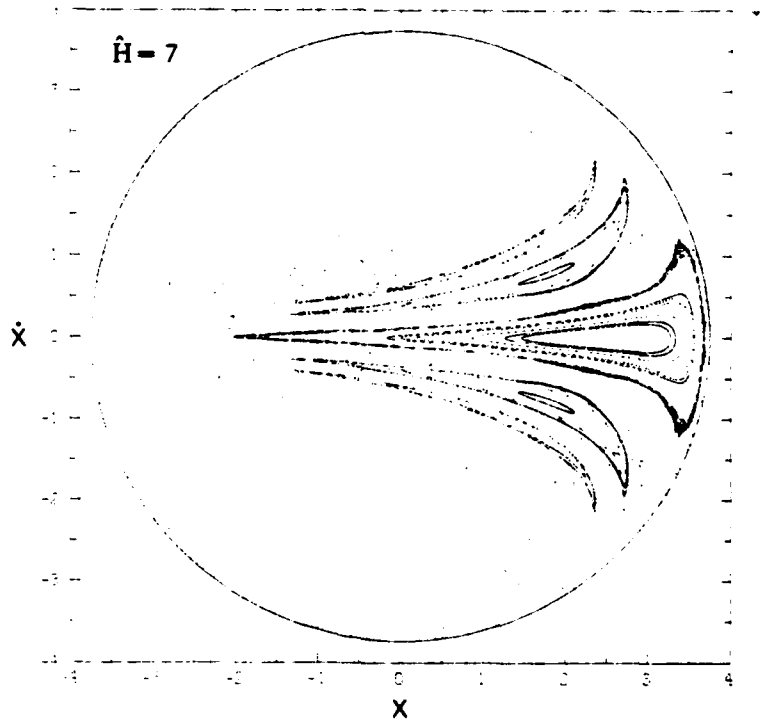

(b) $\hat{H} = 7$

Fig. 3. Surface of section plots. The plots show 40000 to 60000 points.

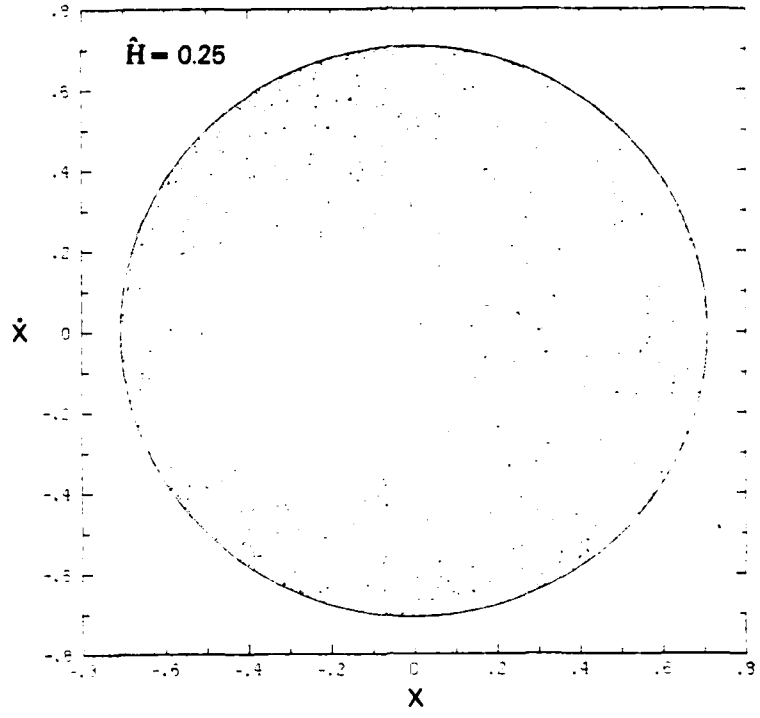

(c) $\hat{H}$ = 0.25

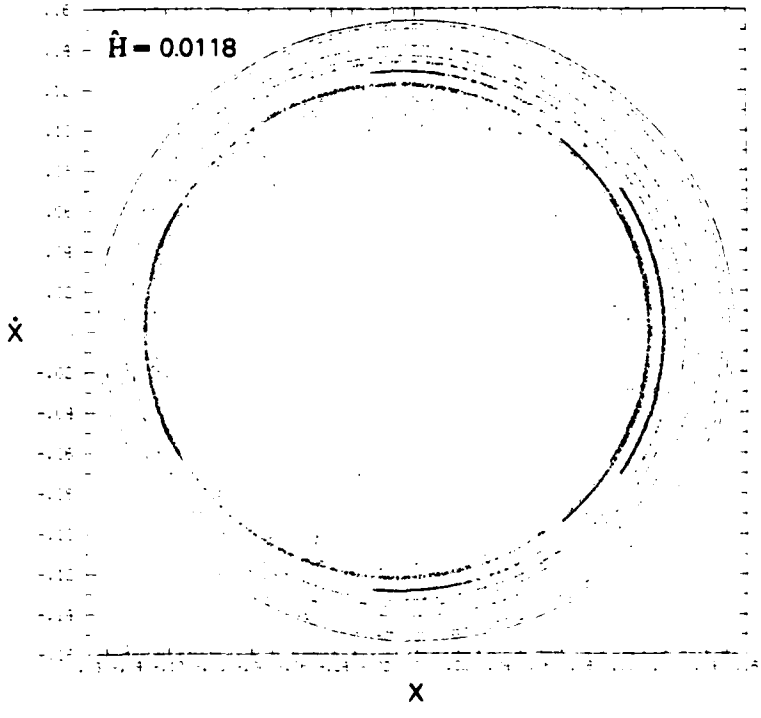

(d) $\hat{H} = 1.184 \times 10^{-2}$

Fig. 3. (Cont'd) Surface of section plots. The plots show 40000 to 60000 points.

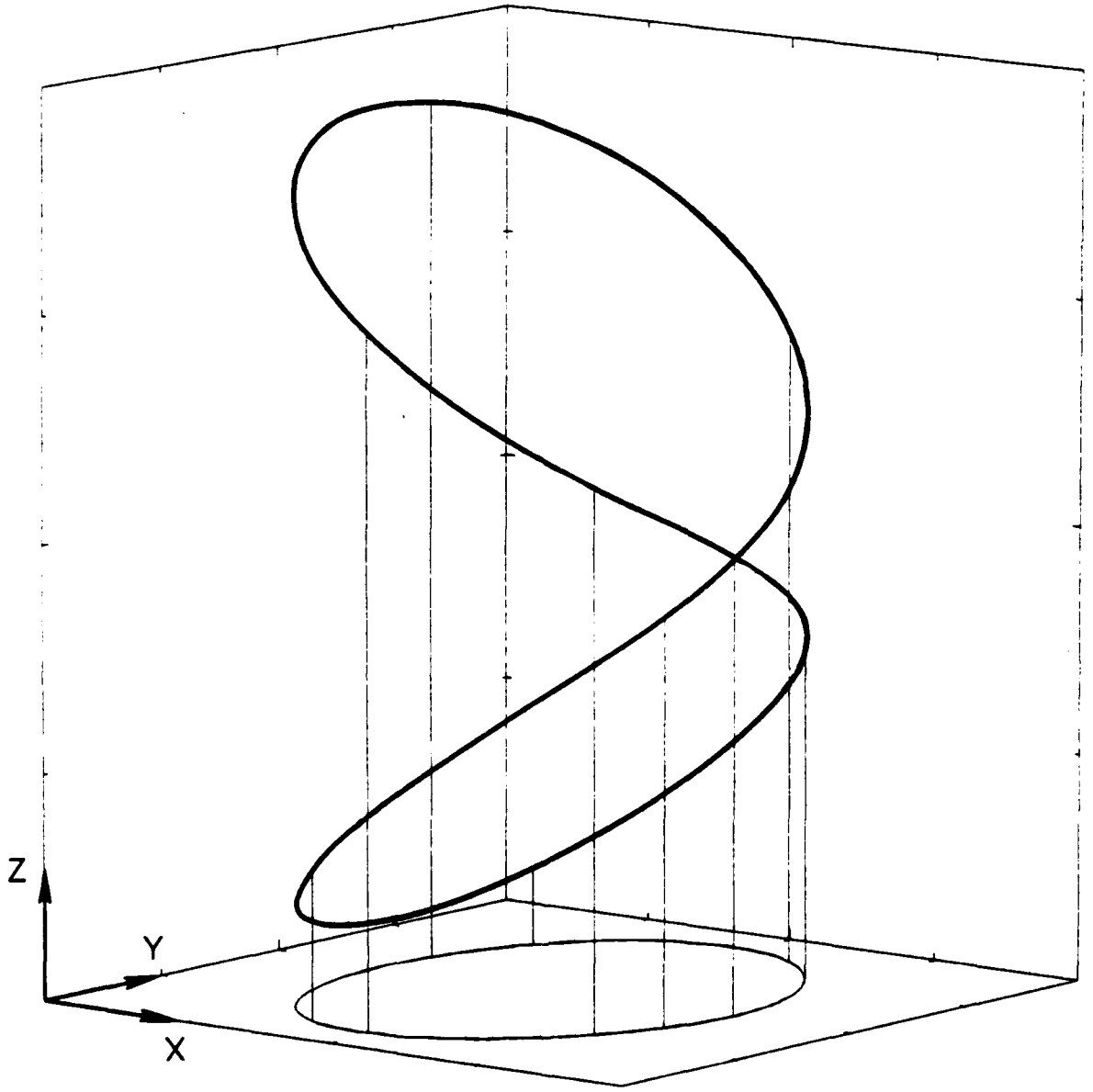

Fig. 4. Three-dimensional displays of selected orbits for $\hat{H} = 500$ and $b_n = 0.1$ (see Figure 2(a)). (a) A fixed point orbit corresponding to X = 22.591 and X = 0. The X - Y - axes have been expanded by factors of 10 and 2, respectively. (b) A transient orbit corresponding to X = 0 and X = -26. The Z - axis has been expanded by a factor of 1.2.

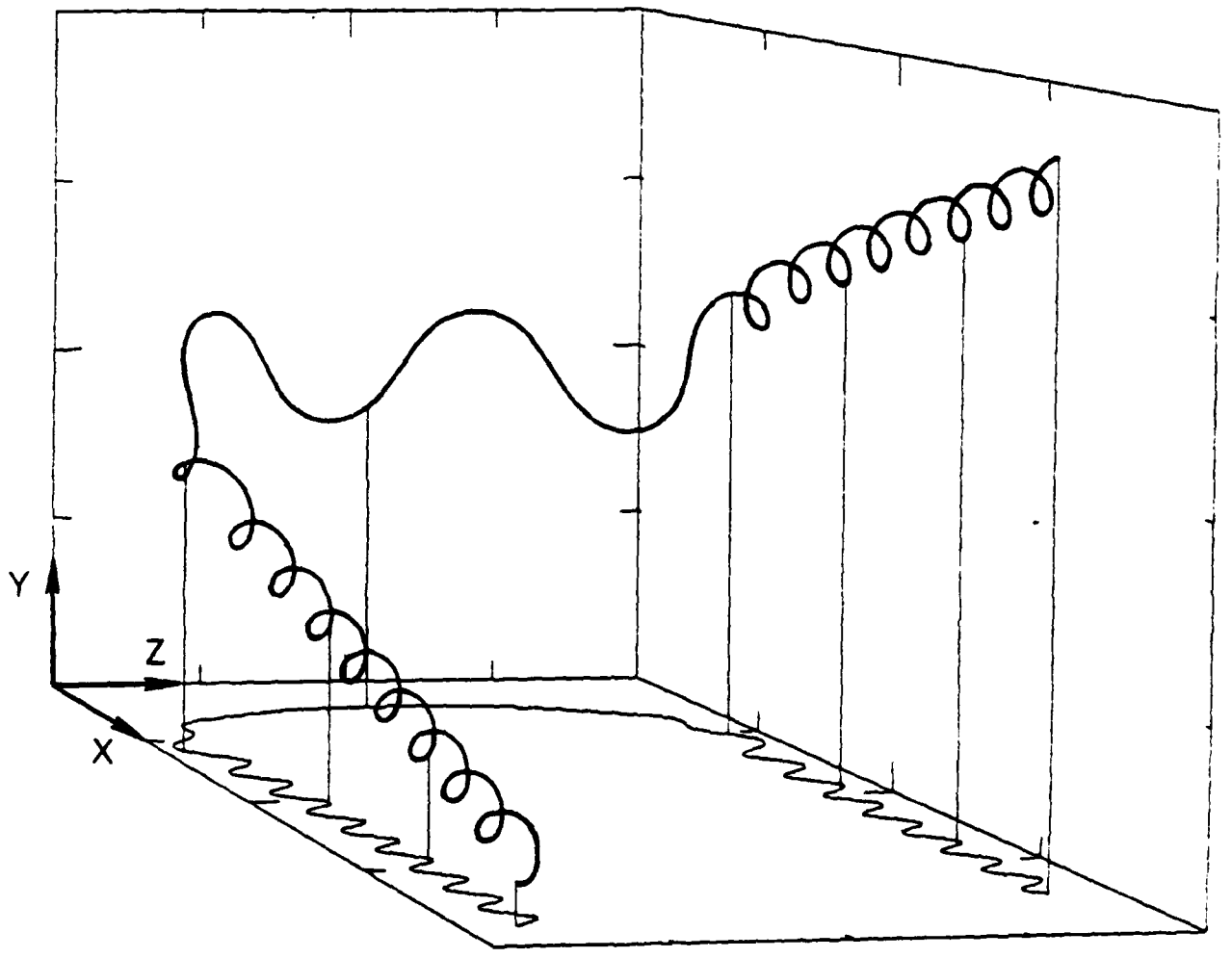

Fig. 4. Cont'd Three dimensional displays of selected orbits for $\hat{H} = 500$ and $b_n = 0.1$ (see Figure 2(a)). (a) A fixed point orbit corresponding to X = 22.591 and X = 0. the X - and Y - axes have been expanded by factors of 10 and 2, respectively. (b) A transient orbit corresponding to X = 0 and X = -26. The Z - axis has been expanded by a factor of 1.2.

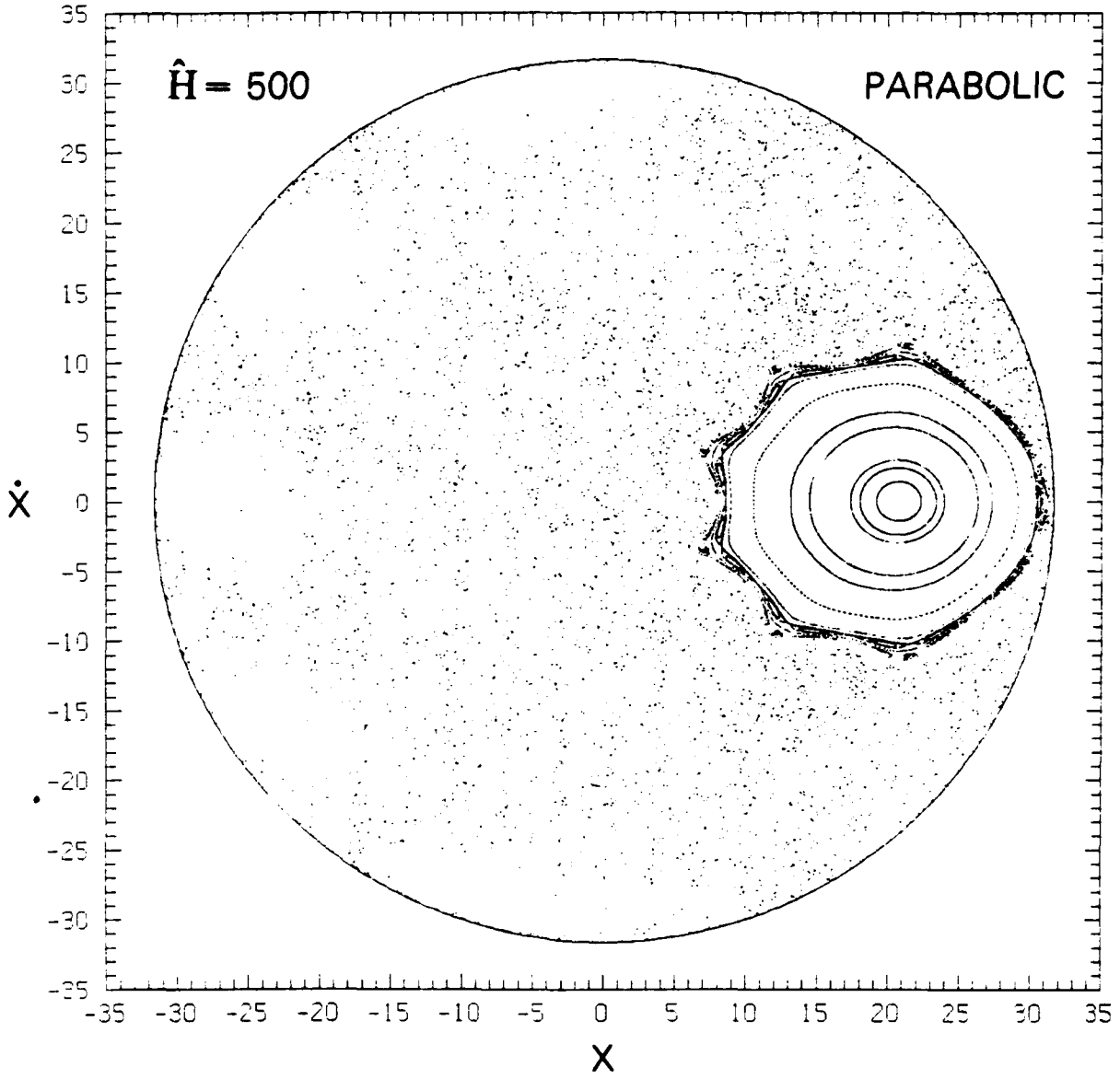

Fig 5. Surface of section plot for the "parabolic" field with $\hat{H} = 500$. 67000 points.

References

Alekseyev, I.I. and A.P. Kropotkin, Interaction of energetic particles with the neutral layer of the tail of the magnetosphere, Geomagn. Aerono., 10, 615, 1970.

Chen, J. and P. Palmadesso, Tearing instability in an anisotropic neutral sheet, Phys. Fluids, 27, 1198, 1984.

Chen, J. and P. Palmadesso, J.A. Fedder and J.G. Lyon, Fast collisionless tearing in an anisotropic neutral sheet, Geophys. Res. Lett. 11, 12, 1984.

Chen, J. and Y.C. Lee, Collisionless tearing instability in a non-Maxwelllian neutral sheet: An integro-differential formulation, Phys. Fluids, 28, 2137, 1985.

Cowley, S.W.H., The adiabatic flow model of a neutral sheet, Cosmic Electrodynamics, 2, 90, 1971.

Eastwood, J.W., Consistency of fields and particle motion in the 'Speiser' model of the current sheet, Plant. Space Sci., 20, 1555, 1972

Furth, H.P., The "mirror instability" for finite particle gyroradius, Nuc. Fusion Suppl. Pt. 1, 169, 1962.

Laval, G., R. Pellat and M. Vuillemin, Instabilities electromagnetiques des plasmas sans collisions, in Plasma Physics and Controlled Nuclear Fusion Research (International Atomic Energy Agency, 1966), Vol. 2.

Lembege, B. and R. Pellat, Stability of a thick two-dimensional quasineutral sheet, Phys. Fluids, 25, 1995, 1982.

Lichtenberg, A.J. and M.A. Lieberman, Regular and Stochastic Motion (Springer-Verlag, New York,1983).

Pellat, R. and G. Schmidt, Absence of particle drift in magnetic fields of translational symmetry, Phys. Fluids, 22, 381, 1979.

Sonnerup, B.U.Ö., Adiabatic particle orbits in a magnetic null sheet, J. Geophys. Res., 76, 8211, 1971.

Speiser, T.W., Particle trajectories in model current sheets, 1. Analytical Solutions, J. Geophys. Res., 70, 4219, 1965.

Speiser, T.W., Particle trajectories in model current sheets, 2. Applications to auroras using geomagnetic tail model, J. Geophys. Res., 72, 3919, 1967.

Speiser, T.W. and L.R. Lyons, Comparison of an analytical approximation for

particle motion in a current sheet with precise numerical calculations, J. Geophys. Res., 89, 147, 1984.

Stern, D. and P. Palmadesso, Drift-free magnetic geometries in adiabatic motion, J. Geophys. Res., 80, 4244, 1975.

Störmer, C., The Polar Aurora", Oxford University Press, London, 1955.

Swift, D., The effect of the neutral sheet on magnetospheric plasma, J. Geophys. Res., 82, 1288, 1977.

Wagner, J.S., J.R. Kan, and S.-I. Akasofu, Particle dynamics in the plasma sheet, J. Geophys. Res., 84 891, 1979.

Distribution List

Director
Naval Research Laboratory
Washington, DC 20375
ATTN: Code 4700 (26 Copies)
Code 4701
Code 4780 (50 copies)
Code 4706 (P. Rodriguez)
Code 2628 (22 copies)
Code 1220 (1 copy)

University of Alaska
Geophysical Institute
Fairbanks, AK 99701
ATTN: Library
S. Akasofu
J. Kan
J. Roederer
L. Lee
D. Swift

University of Arizona
Dept. of Planetary Sciences
Tucson, AZ 85721
ATTN: J.R. Jokipii

University of California, S.D.
LaJolla, CA 92037
(Physics Dept.):
ATTN: T. O'Neil
J. Winfrey
Library
J. Malmberg
(Dept. of Applied Sciences):
ATTN: H. Booker

University of California
Physics Department
Irvine, CA 92664
ATTN: Library
G. Benford
N. Rostoker
C. Robertson
N. Rynn

University of Chicago
Enrico Fermi Institute
Chicago, IL 60637
ATTN: E.N. Parker
I. Lerche
Library

University of California
Los Angeles, CA 90024
(Physic Dept.):
ATTN: J.M. Dawson
B. Fried
J. Maggs
J.G. Moralles
W. Gekelman
R. Stenzel
Y. Lee
A. Wong
F. Chen
M. Ashour-Abdalla
Library
J.M. Cornwall
R. Walker
P. Pritchett

(Institute of Geophysics and
Planetary Physics):
ATTN: Library
C. Kennel
F. Coroniti

Thayer School of Engineering
Dartmouth College
Hanover, NH 03755
ATTN: Bengt U.O. Sonnerup
M. Hudson

University of Colorado
Dept. of Astro-Geophysics
Boulder, CO 80302
ATTN: M. Goldman
Library

Cornell University
School of Applied and Engineering Physics
College of Engineering
Ithaca, NY 14853
ATTN: Library
R. Sudan
B. Kusse
H. Fleischmann
C. Wharton
F. Morse
R. Lovelace
P.M. Kintner

Harvard University
Center for Astrophysics
60 Garden Street
Cambridge, MA 02138
ATTN: G.B. Field
R. Rosner
K. Tsinganos
G.S. Vaiana

University of Iowa
Iowa City, IA 52240
ATTN: C.K. Goertz
D. Gurnett
G. Knorr
D. Nicholson
C. Grabbe
L.A. Frank
K. Nishikawa
N. D'Angelo
R. Merlino
C. Huang

University of Maryland
Physics Dept.
College Park, MD 20742
ATTN: K. Papadopoulos
H. Rowland
C. Wu
L. Vlahos

University of Michigan
Ann Arbor, MI 48140
ATTN: E. Fontheim

University of Minnesota
School of Physics
Minneapolis, MN 55455
ATTN: Library
Dr. J.R. Winckler
Dr. P. Kellogg
Dr. R. Lysak

M.I.T.
Cambridge, MA 02139
ATTN: Library
(Physics Dept.):
ATTN: B. Coppi
V. George
G. Bekefi
T. Chang
T. Dupree
R. Davidson
(Elect. Engineering Dept.):
ATTN: R. Parker
A. Bers
L. Smullin
(R.L.E.):
ATTN: Library
(Space Science):
ATTN: Reading Room

Princeton University
Princeton, NJ 08540
Attn: Physics Library
Plasma Physics Lab. Library
F. Perkins
T.K. Chu
H. Okuda
H. Hendel
R. White
R. Kurlsrud
H. Furth
S. Yoshikawa
P. Rutherford

Rice University
Houston, TX 77001
Attn: Space Science Library
T. Hill
R. Wolf
P. Reiff
G.-H. Voigt

University of Rochester
Rochester, NY 14627
ATTN: A. Simon

Stanford University
Radio Science Lab
Stanford, CA 94305
ATTN: R. Helliwell

Stevens Institute of Technology
Hoboken, NJ 07030
ATTN: B. Rosen
G. Schmidt
M. Seidl

University of Texas
Austin, TX 78712
ATTN: W. Drummond
V. Wong
D. Ross
W. Horton
D. Choi
R. Richardson
G. Leifeste

Lawrence Livermore Laboratory
University of California
Livermore, CA 94551
ATTN: Library
B. Kruer
J. DeGroot
B. Langdon
R. Briggs
D. Pearlstein

Los Alamos National Laboratory
P.O. Box 1663
Los Alamos, NM 87545
ATTN: Library
S.P. Gary
N. Quest
J. Brackbill
J. Birn
J. Borovsky
D. Forslund
J. Kindel
B. Bezzerides
C. Nielson
E. Lindman
L. Thode
D. Winske

Sandia Laboratories
Albuquerque, NM 87115
ATTN: A. Toepfer
D. VanDevender
J. Freeman
T. Wright

Bell Laboratories
Murray Hill, NJ 07974
ATTN: A. Hasegawa
L. Lanzerotti

Lockheed Research Laboratory
Palo Alto, CA 94304
ATTN: M. Walt
J. Cladis
Y. Chiu
R. Sharp
E. Shelley

Physics International Co.
2400 Merced Street
San Leandro, CA 94577
ATTN: J. Benford
S. Putnam
S. Stalings
T. Young

Science Applications, Inc.
Lab. of Applied Plasma Studeis
P.O. Box 2351
LaJolla, CA 92037
ATTN: L. Linson

NASA/Goddard Space Flight Center
Greenbelt, MD 20771
ATTN: M. Goldstein
T. Northrop
T. Birmingham

NASA/Goddard Space Flight Center
Greenbelt, MD 20771
ATTN: A. Figuero Vinas
Code 692

TRW Space and Technology Group
Space Science Dept.
Building R-1, Room 1170
One Space Park
Redondo Beach, CA 90278
ATTN: R. Fredericks
W.L. Taylor

National Science Foundation
Atmospheric Research Section (ST)
Washington, DC 20550
ATTN: D. Peacock

Goddard Space Flight Center
Code 961
Greenbelt, MD 20771
ATTN: Robert F. Benson

NASA Headquarters
Code EE-8
Washington, DC 20546
ATTN: Dr. S. Shawhan
Dr. D. Butler

Klumpar, David
Center for Space Sciences
P.O Box 688
University of Texas
Richardson, TX 75080

Aerospace Corp.
A6/2451, P.O. Box 92957
Los Angeles, CA 90009
ATTN: A. Newman
D. Gorney
M. Schulz
J. Fennel

Space Science Lab.
University of California
Berkeley, CA 94720
ATTN: M. Temerin
F. Mozer

IPST
University of Maryland
College Park, MD 20742
ATTN: David Matthews

Utah State University
Dept. of Physics
Logan, UT 84322
ATTN: Robert W. Schunk

Director
Defense Nuclear Agency
Washington, DC 20305
ATTN: Dr. Leon Wittwer
Dr. P. Crowley

Office of Naval Research
Washington, DC 22170
ATTN: Dr. C. Roberson
(Code 412)

Commanding Officer
Office of Naval Research Western
Regional Office
1030 East Green Street
Pasadena, CA 91106
ATTN: R. Brandt

Boston College
Department of Physics
Chestnut Hill, MA 02167
ATTN: R.L. Carovillano
P. Bakshi

University of New Hampshire
Department of Physics
Durham, NH 03824
ATTN: R.L. Kaufmann
J. Hollweg

Director of Research
U.S. Naval Academy
Annapolis, MD 21402 (2 copies)

END

FILMED

1-86

DTIC